ARTICLE

doi:10.1038/nature22337

A *Cryptosporidium* PI(4)K inhibitor is a drug candidate for cryptosporidiosis

Ujjini H. Manjunatha[1]*, Sumiti Vinayak[2]*, Jennifer A. Zambriski[3]*, Alexander T. Chao[1], Tracy Sy[3], Christian G. Noble[1], Ghislain M. C. Bonamy[1], Ravinder R. Kondreddi[1], Bin Zou[1], Peter Gedeck[1], Carrie F. Brooks[2], Gillian T. Herbert[2], Adam Sateriale[2], Jayesh Tandel[4], Susan Noh[3,5,6], Suresh B. Lakshminarayana[1], Siau H. Lim[1], Laura B. Goodman[7], Christophe Bodenreider[1], Gu Feng[1], Lijun Zhang[8], Francesca Blasco[1], Juergen Wagner[1], F. Joel Leong[1], Boris Striepen[2,4] & Thierry T. Diagana[1]

Diarrhoeal disease is responsible for 8.6% of global child mortality. Recent epidemiological studies found the protozoan parasite *Cryptosporidium* to be a leading cause of paediatric diarrhoea, with particularly grave impact on infants and immunocompromised individuals. There is neither a vaccine nor an effective treatment. Here we establish a drug discovery process built on scalable phenotypic assays and mouse models that take advantage of transgenic parasites. Screening a library of compounds with anti-parasitic activity, we identify pyrazolopyridines as inhibitors of *Cryptosporidium parvum* and *Cryptosporidium hominis*. Oral treatment with the pyrazolopyridine KDU731 results in a potent reduction in intestinal infection of immunocompromised mice. Treatment also leads to rapid resolution of diarrhoea and dehydration in neonatal calves, a clinical model of cryptosporidiosis that closely resembles human infection. Our results suggest that the *Cryptosporidium* lipid kinase PI(4)K (phosphatidylinositol-4-OH kinase) is a target for pyrazolopyridines and that KDU731 warrants further preclinical evaluation as a drug candidate for the treatment of cryptosporidiosis.

Infections that cause diarrhoea are responsible for nearly 800,000 deaths every year, mostly among young children in resource-poor settings[1]. Recently, the apicomplexan parasite *Cryptosporidium* was found to be one of the leading causes of infectious diarrhoea in children[2,3], and infection with this parasite is strongly associated with mortality, growth stunting, and developmental deficits[4]. The major human pathogens causing cryptosporidiosis, *C. hominis* and *C. parvum*, infect the epithelial cells of the intestine and, through a mechanism that is not fully understood, trigger severe watery diarrhoeal symptoms. These are particularly long-lasting and often life-threatening in malnourished and immunocompromised children[4]. Nitazoxanide, the only approved drug for the treatment of cryptosporidiosis, has limited efficacy in these most vulnerable patient populations[5,6]. Cryptosporidiosis is also a well-recognized opportunistic infection in adults with AIDS and transplant recipients[4]. Infection occurs through ingestion of the spore-like oocyst stage, which shows remarkable resistance to water chlorination. Therefore, even in countries that apply advanced water treatment, infection is common, and *Cryptosporidium* is the cause of 50% of disease outbreaks linked to recreational water use in the USA. The search for cryptosporidiosis therapeutics has been hindered by the many technical challenges faced when working with this notoriously intractable parasite[7]. Here we establish a drug-discovery screening process for cryptosporidiosis that combines phenotypic *in vitro* assays with novel animal models that take advantage of transgenic parasites[8].

Cryptosporidium compound screen

To discover new treatments for cryptosporidiosis, we assembled a set of 6,220 compounds with known activity against various protozoan parasites and screened them against *C. parvum* in a high-content imaging infection assay in HCT-8 cells (see Supplementary Information). Notably, many anti-malarials (spiroindolones[9], cyclomarins[10], and imidazolopiperazines[11]) lacked activity against *Cryptosporidium*; however, 154 compounds showed >60% growth inhibition at 5 μM. Secondary screening using a novel cytopathic effect (CPE)-based *C. parvum* assay confirmed several scaffolds, with imidazopyrazines[12,13] and pyrazolopyridines[14] showing sub-micromolar cellular activity (Fig. 1a–d and Table 1; structures provided in Extended Data Fig. 1). We evaluated about 200 pyrazolopyridine analogues and found correlation between activity against *C. parvum* and *Plasmodium falciparum* ($r^2 = 0.702$; Fig. 1d), suggesting that the mechanism of action of pyrazolopyridines is conserved between these two parasites. No such correlation was observed with toxicity against HepG2 ($r^2 = 0.071$) (Extended Data Fig. 2). *C. hominis* is responsible for most clinical infections[15]. We thus evaluated a subset of pyrazolopyridine analogues against *C. hominis*, and found potency comparable to that against *C. parvum* ($r^2 = 0.872$; Fig. 1e and Table 1).

Pyrazolopyridines inhibit CpPI(4)K

Knowing that pyrazolopyridines and imidazopyrazines exert their antimalarial activity through inhibition of the *Plasmodium* lipid kinase PI(4)K[12,16], we searched for potential *Cryptosporidium* orthologues. The genomes of both *C. parvum* and *C. hominis* encode multiple putative lipid kinases, and the PI(4)K catalytic domain of cgd8_4500 and its *C. hominis* homologue Chro.80518 show 71.8% amino-acid sequence similarity to *P. falciparum* PI(4)K. We expressed cgd8_4500 in insect cells and purified the protein (CpPI(4)K), which displays phosphatidylinositol kinase activity with a Michaelis constant (K_m) for ATP and phosphatidylinositol of 3 and 0.4 μM, respectively (Extended Data Fig. 3). Using this assay, we showed that the imidazopyrazine KDU691 and the pyrazolopyridine KDU731 are potent inhibitors of CpPI(4)K

[1]Novartis Institute for Tropical Diseases, 10 Biopolis Road, 05-01 Chromos, Singapore 138670, Singapore. [2]Center for Tropical and Emerging Global Diseases, University of Georgia, Athens, Georgia 30602, USA. [3]Washington State University, College of Veterinary Medicine, Paul G. Allen School for Global Animal Health, Pullman, Washington 99164, USA. [4]Department of Cellular Biology, University of Georgia, Athens, Georgia 30602, USA. [5]USDA-Agricultural Research Service, Animal Disease Research Unit, Washington State University, Pullman, Washington 99164, USA. [6]Washington State University, Department of Veterinary Microbiology and Pathology, Washington Animal Disease Diagnostic Laboratory, Pullman, Washington, USA. [7]Cornell University, College of Veterinary Medicine, Department of Population Medicine and Diagnostic Sciences, Ithaca, New York 14853, USA. [8]China Novartis Institutes for Biomedical Research, Zhangjiang Hi-Tech Park, Pudong, Shanghai 201203, China.
*These authors contributed equally to this work.

© 2017 Macmillan Publishers Limited, part of Springer Nature. All rights reserved.

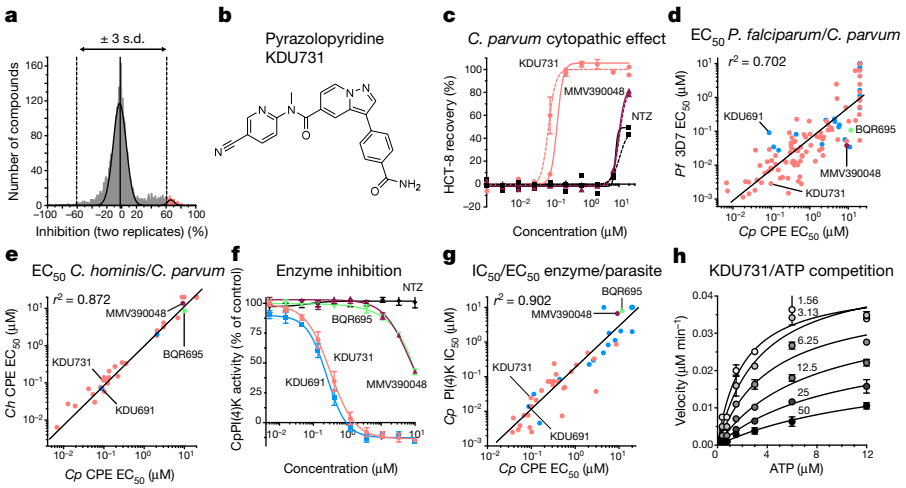

Figure 1 | Pyrazolopyridine analogues exhibit potent anti-*Cryptosporidium* activity. a, *C. parvum* phenotypic screening against a focused library of 6,220 compounds (percentage inhibition at 5 μM). Hits with inhibition >3 s.d. are shown in red. **b**, Structure of the pyrazolopyridine lead KDU731. **c**, *In vitro* activity of KDU731 (red), MMV3900048 (maroon), and nitazoxanide (NTZ, black) against *C. parvum* (solid line) and *C. hominis* (dashed line). **d**, Correlation of growth inhibition (EC_{50}) of selected compounds between *C. parvum* (*Cp*) and *P. falciparum* (*Pf*). Pyrazolopyridine analogues are shown in red, imidazopyrazines in blue, quinoxaline in green, and diaryl-aminopyridine in maroon. **e**, Correlation of growth inhibition (EC_{50}) between *C. parvum* and *C. hominis* (*Ch*) for selected compounds. **f**, Inhibition of phosphatidylinositide kinase activity of purified enzyme by KDU731, KDU691, MMV390048, and BQR695 (means ± s.e.m. with at least three biological replicates) in the presence of 3 μM ATP. **g**, Correlation between inhibition of PI kinase activity of purified CpPI(4)K enzyme (IC_{50}) and growth inhibition (EC_{50}) of *C. parvum* with selected compounds (colours as in **d**). **h**, CpPI(4)K activity across a range of ATP concentrations in the presence of 1.56–50 nM KDU731. Data shown in **c** and **f** represent mean ± s.e.m., $n = 3$ biological replicates, representative data shown. Experiments shown in **d**, **e**, and **g** were repeated at least twice and geometric mean EC_{50} values are plotted; experiment in **h** was repeated twice (biological replicates) and one representative assay is shown. (Error bars are from the technical replicate, $n = 2$.)

enzymatic activity with half-maximal inhibitory concentration (IC_{50}) values of 17 and 25 nM, respectively (Fig. 1f). Both compounds have a >50-fold selectivity window against the human PI(4)K IIIβ homologue (Extended Data Table 1).

When we measured diverse imidazopyrazine and pyrazolopyridine analogues against CpPI(4)K enzymatic activity and *C. parvum* growth in cells, we found a tight correlation ($r^2 = 0.902$) (Fig. 1g), suggesting that the anti-*Cryptosporidium* activity is directly mediated by CpPI(4)K inhibition. Further genetic and structural insights are needed to unambiguously establish PI4(K) as the target. However, we note that the *Plasmodium* PI(4)K inhibitors diaryl-aminopyridine (MMV390048)[17] and quinoxaline (BQR695)[12], which are inactive against *C. parvum* and *C. hominis*, do not inhibit CpPI(4)K enzymatic activity (Fig. 1f). Finally, mechanistic studies revealed an increased K_m for ATP in the presence of KDU731 (Fig. 1h), suggesting ATP-competitive inhibition similar to that previously observed for the *Plasmodium* enzyme[12]. Additional structure–activity relationship analysis of pyrazolopyridines against *Cryptosporidium* is found in the Supplementary Information. Taken together, our data suggest that pyrazolopyridines are inhibitors of CpPI(4)K that bind to the ATP-binding site of the enzyme with a favourable selectivity window over human PI(4)K.

Pharmacokinetic properties of KDU731

The most urgent need for effective cryptosporidiosis treatment is among children under the age of 2 years. A very safe drug profile is thus a key component of the target product profile[18,19]. KDU731 has a selectivity index of more than 100 (half-maximal cytotoxicity concentration (CC_{50}) of HepG2 = 15.6 μM and half-maximal effective concentration (EC_{50}) of *C. parvum* CPE = 0.1 μM) (Extended Data Table 1). In a battery of safety pharmacology assays, the compound does not show intrinsic risks for cardiotoxicity, mutagenicity, clastogenicity, or phototoxicity, and it does not bind significantly to a panel of human anti-targets (Extended Data Tables 1 and 2). KDU731 safety was further evaluated in a 2-week toxicology study in rats using a solid dispersion formulation to maximize systemic exposure (~25-fold). In this study, no significant histopathological changes and only minor changes in clinical chemistry and haematology were observed (slight elevation of cholesterol and phosphate

Table 1 | Activity of pyrazolopyridine analogues and other known PI(4) kinase inhibitors

Compound	*Cp* CPE EC_{50} (μM)	*Cp* HCI IC_{50} (μM)	*Ch* CPE EC_{50} (μM)	*Cp* PI(4)K IC_{50} (μM)	*Pf* 3D7 IC_{50} (μM)	HepG2 CC_{50} (μM)
KDU731	0.107 ± 0.039	0.063 ± 0.028	0.130 ± 0.074	0.025 ± 0.004	0.003 ± 0.001	15.621 ± 8.621
KDU691	0.096 ± 0.044	0.054 ± 0.029	0.082 ± 0.017	0.017 ± 0.012	0.108 ± 0.061	27.291 ± 14.169
MMV390048	12.792 ± 6.264	13.422	11.85 ± 2.758	8.335 ± 2.355	0.042 ± 0.022	26.156 ± 16.063
BQR695	11.837 ± 1.889	8.344	8.565	7.305 ± 0.841	0.118 ± 0.055	26.711 ± 13.870
Nitazoxanide	14.286 ± 7.127	2.927 ± 0.808	>20.000	>10.000	>10.000	12.749 ± 2.378
KDU370	1.540	ND	2.543	0.212	0.074 ± 0.032	>50.000
KDZ464	0.113 ± 0.072	0.232	0.119	0.003	0.005 ± 0.001	21.222 ± 10.594
LNN134	1.951 ± 0.340	1.031	1.937	0.488	0.126 ± 0.115	40.025 ± 17.278
LMW740	>20.000	>20.000	>20.000	>10.000	0.521	>50.000
KEL204	>20.000	>20.000	>20.000	3.701	1.432	>50.000

Cp, *C. parvum*; *Ch*, *C. hominis*; *Pf*, *P. falciparum*; HCI; high-content imaging assay. ND, not determined. Data shown are means ± s.e.m., $n = 3$ biological replicates.

© 2017 Macmillan Publishers Limited, part of Springer Nature. All rights reserved.

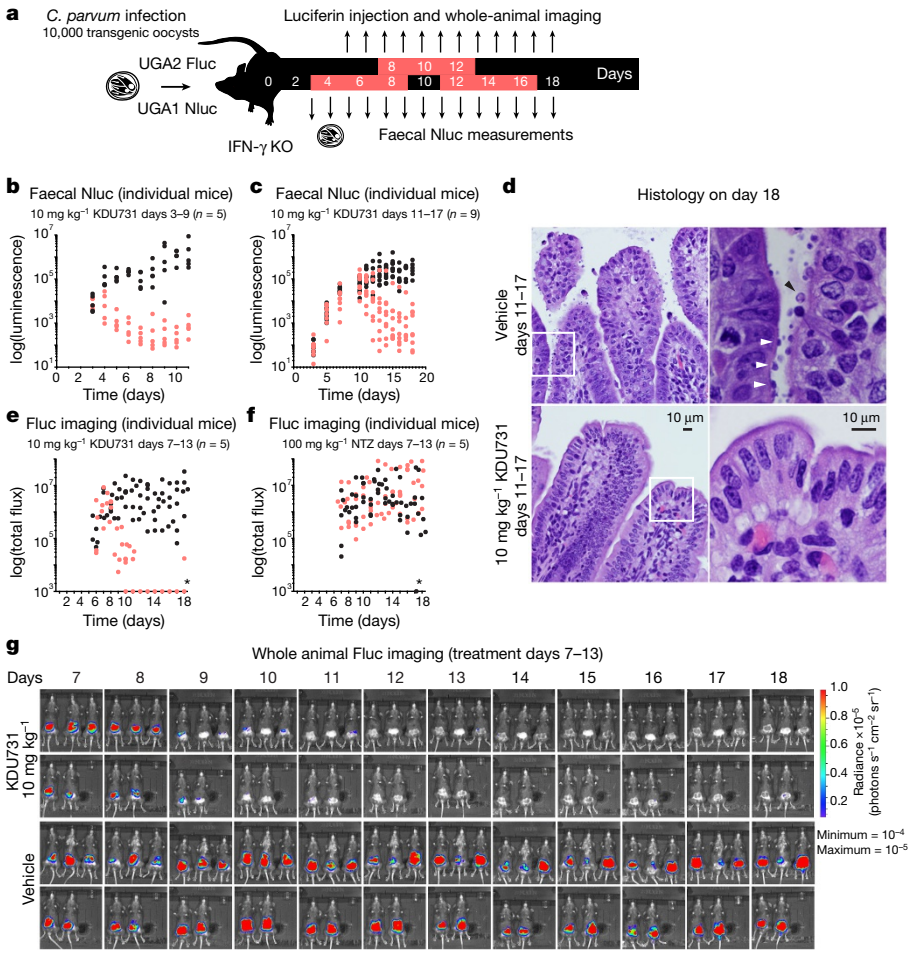

Figure 2 | KDU731 has potent activity against *Cryptosporidium* in immunocompromised IFN-γ knockout mice. a, Mice were infected with 10,000 *C. parvum* UGA1 Nluc or UGA2 Fluc oocysts. Parasite load in the faeces was determined by measuring faecal Nluc activity and parasite tissue load was quantified by whole-animal imaging of Fluc activity. Different 7-day treatment courses are indicated in red. Faecal luciferase measurements of individual mice with treatment initiated after 3 (**b**) or 11 (**c**) days of infection (red; vehicle control shown in black), $n = 5$ and $n = 9$ mice respectively, representative of two biological replicates for **b** and **c**. **d**, Histology of the ileum of infected mice (shown in **c**) after 1 week of KDU731 treatment compared with vehicle-treated control on day 18 ($n = 3$ biological replicates, representative images shown here). Note numerous intracellular parasite stages (white arrowheads) and extracellular oocysts (black arrowhead) in the control, absent in the treated mice. Vehicle-treated animals showed disorganized columnar epithelial cells and loss of brush border compared with KDU731-treated mice. White box indicates section shown at higher magnification to the right. Mice ($n = 5$) infected with UGA2 FLuc were treated on day 7 with 10 mg per kg (body weight) of KDU731 (red, **e** and **g**), 100 mg per kg (body weight) nitazoxanide (red, **f**; also see Extended Data Fig. 6), or vehicle (black, **e** and **f**) for 1 week. Animals were monitored by whole-animal imaging and a radiance scale and quantification of total flux in photons per second is shown. *Animals shown on the baseline were below the level of detection.

ions and increase in red blood cells, see Supplementary Information). Importantly, no haematopoietic toxicity related to potential inhibition of PI3K or PI4K lipid kinases was observed, suggesting that the *in vitro* selectivity of KDU731 translated to lack of host toxicity *in vivo* (Extended Data Table 1). Children with cryptosporidiosis in resource-limited settings frequently suffer comorbidities including HIV, tuberculosis, and other infections; anti-cryptosporidial drugs will thus probably be used along with other medications, and the risk of drug–drug interactions needs to be minimized. Consistent with the requirement, KDU731 did not inhibit any of the major cytochrome P450 isoenzymes and did not induce human pregnane X receptor (Extended Data Table 1).

KDU731 pharmacokinetics, metabolism, and distribution were examined in mice, rats, and rhesus monkeys. Upon intravenous administration, KDU731 displayed a low-to-moderate volume of distribution ($V_{ss} = 1.12$ and $2.15\ l\,kg^{-1}$), a low total systemic clearance (CL = 6.8 and 16 ml $min^{-1}\,kg^{-1}$), and a half-life ranging from 1 to 4 h (Extended Data Table 3). KDU731 orally administered in suspension formulation displayed a moderate half-life ($t_{1/2} = 2$–4 h) in all three species. KDU731 was selected as a drug candidate because it shows moderate-to-low oral bioavailability (37% in rodents, 9% in non-human primates). As *Cryptosporidium* primarily infects the intestinal epithelium, we reasoned that systemic exposure may not be required for efficacy and that limiting systemic exposure may further enhance the safety margin of a cryptosporidiosis drug.

KDU731 treatment of infected mice

Current assessment of cryptosporidiosis treatments relies on laborious methods to quantify the parasite in animals. We used genetically modified parasites to build more facile models. We established the EC_{50} of KDU731 for transgenic parasites[8] in HCT-8 using Nanoluciferase (Nluc) as a readout and found it comparable to the EC_{50} for wild-type parasites (Extended Data Fig. 4a). Next, we inoculated 6- to 8-week-old C57BL/6 interferon-γ (IFN-γ)-knockout mice with 10,000 oocysts and monitored infection by following parasite-derived luciferase activity in the faeces (Fig. 2a). Infected mice were treated orally with KDU731 in suspension formulation and parasite load was measured in the pooled faeces by Nluc and quantitative PCR (qPCR) assay with a high degree of correlation (Spearman coefficient = 0.786; two-tailed $P = 0.048$). The Nluc assay has a small sample requirement (20 mg) and

© 2017 Macmillan Publishers Limited, part of Springer Nature. All rights reserved.

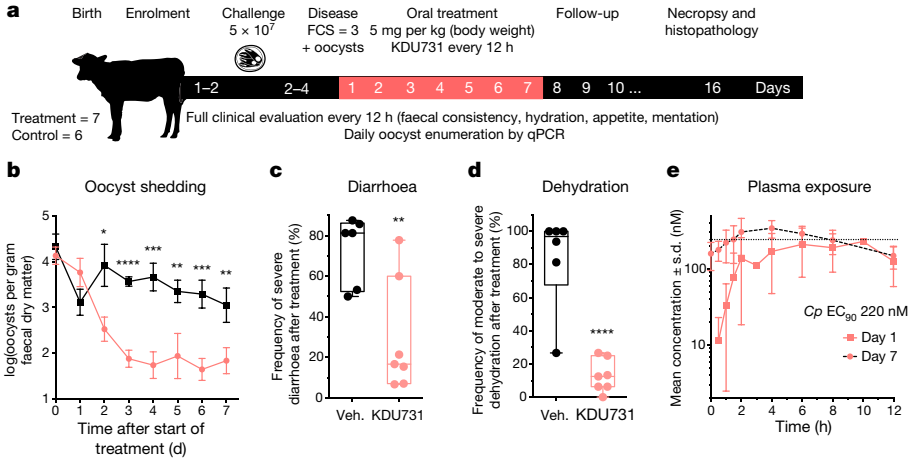

Figure 3 | Therapeutic efficacy of KDU731 in neonatal calf clinical model of cryptosporidiosis. a, Within 48 h of birth, calves were challenged with 5×10^7 *C. parvum* oocysts. Faecal oocyst shedding was enumerated by qPCR and calves were clinically evaluated every 12 h. Oral treatment with KDU731 (5 mg per kg (body weight) every 12 h for 7 days) was initiated when calves showed severe diarrhoea (faecal consistency score (FCS) = 3) and oocysts in their faeces. KDU731-treated calves shed significantly fewer oocysts in their stool (**b**), had significantly fewer days of severe diarrhoea (**c**), and were significantly less dehydrated (**d**) than untreated calves. **e**, Day 1 and day 7 plasma pharmacokinetic profile of KDU731. Data shown here (**b**–**e**) are from infected calves that were treated with vehicle (Veh.) ($n = 6$) or KDU731 ($n = 7$); n represents the number of calves. *In vitro* EC_{90} is shown as dotted line. Error bars, s.e.m. Data shown here (**c**, **d**) as a 'box and whiskers' plot; the box extends from the 25th to 75th percentiles, and whiskers with minimum to maximum showing all data points. Data in **b** and **e** were determined to display non-Gaussian distribution and were log-transformed before statistical analysis using *t*-tests with two-tailed $*P < 0.05$, **0.01, ***0.001, and ****0.0001; data in **c** and **d** were determined to be normally distributed and analysed using *t*-tests.

thus could be conducted on individual mice as well as pooled faeces (unpaired *t*-test comparing means of individual and pooled readings showed no significant difference, two-tailed $P = 0.3862$). Importantly, KDU731 greatly reduced oocyst shedding regardless of assay method (Fig. 2b and Extended Data Fig. 4b, c; non-parametric Kruskal–Wallis test, pooled Nluc two-tailed $P < 0.001$; faecal qPCR two-tailed $P = 0.0042$). In a modified design, KDU731 (10 mg per kg (body weight)) treatment was initiated at the peak of infection, again resulting in a significant reduction in oocyst shedding (Fig. 2a, c). At the end of the treatment period, three mice per group were killed and intestines were processed for histology. We did not observe parasites in the intestines of treated animals, whereas those that received vehicle showed substantial infection (Fig. 2d).

To dynamically evaluate the impact of treatment on parasite load directly in the intestinal tissue, we engineered a new reporter parasite amenable to detection by whole-animal imaging. Mice were infected with parasites expressing red-shifted firefly luciferase[20] (Fluc) and imaged after D-luciferin injection. Intestinal tissue load was quantified by PCR and we found strong correlation with tissue luminescence ($r^2 = 0.8$; Extended Data Fig. 5a, b). KDU731 treatment of mice infected with Fluc parasites was initiated on day 7, when all mice registered high levels of abdominal luciferase activity and mice were imaged daily. Tissue load dropped markedly within 2 days of treatment, and fell below the limit of detection after 5 days (Fig. 2e, g). Changes in luminescence imaging were mirrored by faecal oocyst shedding quantified by PCR (Spearman coefficient = 0.840, two-tailed $P = 0.0006$; Extended Data Fig. 5c). For comparison, we evaluated nitazoxanide at 100 mg per kg (body weight) and observed no change (Fig. 2f and Extended Data Fig. 6), consistent with previous reports on immunosuppressed hosts[5,21].

Treatment of neonatal calves

Newborn calves are naturally susceptible to *C. parvum* infection, resulting in faecal oocyst shedding, profuse watery diarrhoea, and severe dehydration, which closely mirrors human symptomology[22,23]. We challenged 13 neonatal calves with 5×10^7 oocysts. Over the duration of enrolment, a complete physical examination was performed every 12 h and clinical data including appetite, mentation, faecal consistency, and hydration status were recorded (Fig. 3) to assign a clinical score on a scale of 1 (normal) to 3 (severe) in accordance with previously described methods (see rubric in Supplementary Information)[22–24]. Faecal oocyst shedding was enumerated every 24 h by qPCR. The treatment group ($n = 7$) was subjected to oral treatment with 5 mg per kg (body weight) KDU731 in suspension formulation every 12 h for 7 days. Treatment was initiated upon development of fulminant diarrhoea and faecal oocyst shedding, between day 2 and day 4 after infection.

All calves tolerated KDU731 treatment without compound-related abnormalities, and treated calves shed significantly fewer oocysts than vehicle-treated calves within 3 days of treatment ($P < 0.0001$ on day 3) (Fig. 3b). Treated calves suffered fewer days of severe diarrhoea (two-tailed $P = 0.006$) and were significantly less dehydrated (two-tailed $P < 0.0001$) than controls (Fig. 3c, d). Resolution of clinical signs started as early as 24 h after treatment was initiated. Within 48 h of treatment, six out of seven calves showed no signs of dehydration, and within 72 h of treatment five of six calves had resolution of severe diarrhoea (Extended Data Fig. 7). KDU731 displayed limited systemic exposure in calves with a maximum serum concentration (C_{max}) and an absorption (area under the concentration–time curve, AUC) of 0.228 μM and 1.9 μM h^{-1} respectively (Fig. 3e and Extended Data Table 3), confirming that substantial systemic exposure may not be required for parasite clearance and resolution of clinical illness.

Conclusions

Our studies define the pyrazolopyridine KDU731 as a promising anti-cryptosporidial drug candidate that is active against both *C. parvum* and *C. hominis*. Unlike nitazoxanide, KDU731 demonstrated *in vivo* efficacy in immunocompromised mice. Additionally, treatment in neonatal calves, which closely matches the pathophysiological and pharmacological challenges faced in the treatment of young malnourished children, led to a significant decrease in parasite shedding and rapid resolution of diarrhoea and dehydration. Our lead candidate, KDU731, displays good anti-cryptosporidial activity and meets a broad range of safety and pharmacology criteria required for a much-needed novel cryptosporidiosis therapeutic intervention. Further safety and pharmacological preclinical evaluation is currently ongoing to support the initiation of human clinical trials.

© 2017 Macmillan Publishers Limited, part of Springer Nature. All rights reserved.

Online Content Methods, along with any additional Extended Data display items and Source Data, are available in the online version of the paper; references unique to these sections appear only in the online paper.

Received 27 November 2016; accepted 31 March 2017.
Published online 31 May 2017.

1. Liu, L. *et al.* Global, regional, and national causes of under-5 mortality in 2000–15: an updated systematic analysis with implications for the Sustainable Development Goals. *Lancet* **388,** 3027–3035 (2016).
2. Kotloff, K. L. *et al.* Burden and aetiology of diarrhoeal disease in infants and young children in developing countries (the Global Enteric Multicenter Study, GEMS): a prospective, case-control study. *Lancet* **382,** 209–222 (2013).
3. Platts-Mills, J. A. *et al.* Pathogen-specific burdens of community diarrhoea in developing countries: a multisite birth cohort study (MAL-ED). *Lancet Glob. Health* **3,** e564–e575 (2015).
4. Checkley, W. *et al.* A review of the global burden, novel diagnostics, therapeutics, and vaccine targets for cryptosporidium. *Lancet Infect. Dis.* **15,** 85–94 (2015).
5. Amadi, B. *et al.* High dose prolonged treatment with nitazoxanide is not effective for cryptosporidiosis in HIV positive Zambian children: a randomised controlled trial. *BMC Infect. Dis.* **9,** 195 (2009).
6. Amadi, B. *et al.* Effect of nitazoxanide on morbidity and mortality in Zambian children with cryptosporidiosis: a randomised controlled trial. *Lancet* **360,** 1375–1380 (2002).
7. Striepen, B. Parasitic infections: time to tackle cryptosporidiosis. *Nature* **503,** 189–191 (2013).
8. Vinayak, S. *et al.* Genetic modification of the diarrhoeal pathogen *Cryptosporidium parvum*. *Nature* **523,** 477–480 (2015).
9. Rottmann, M. *et al.* Spiroindolones, a potent compound class for the treatment of malaria. *Science* **329,** 1175–1180 (2010).
10. Bürstner, N. *et al.* Gift from nature: cyclomarin A kills mycobacteria and malaria parasites by distinct modes of action. *ChemBioChem* **16,** 2433–2436 (2015).
11. Meister, S. *et al.* Imaging of *Plasmodium* liver stages to drive next-generation antimalarial drug discovery. *Science* **334,** 1372–1377 (2011).
12. McNamara, C. W. *et al.* Targeting *Plasmodium* PI(4)K to eliminate malaria. *Nature* **504,** 248–253 (2013).
13. Zou, B. *et al.* Lead optimization of imidazopyrazines: a new class of antimalarial with activity on *Plasmodium* liver stages. *ACS Med. Chem. Lett.* **5,** 947–950 (2014).
14. Chatterjee, A. K. *et al.* Preparation of pyrazolopyridine compounds for the treatment of parasitic diseases. US patent WO 2014078802 A1 (2014).
15. Xiao, L. Molecular epidemiology of cryptosporidiosis: an update. *Exp. Parasitol.* **124,** 80–89 (2010).
16. Zeeman, A. M. *et al.* PI4 kinase is a prophylactic but not radical curative target in *Plasmodium vivax*-type malaria parasites. *Antimicrob. Agents Chemother.* **60,** 2858–2863 (2016).
17. Ghidelli-Disse, S. *et al.* Identification of *Plasmodium* PI4 kinase as target of MMV390048 by chemoproteomics. *Malar. J.* **13** (Suppl. 1), P38 (2014).
18. Huston, C. D. *et al.* A proposed target product profile and developmental cascade for new cryptosporidiosis treatments. *PLoS Negl. Trop. Dis.* **9,** e0003987 (2015).
19. Manjunatha, U. H., Chao, A. T., Leong, F. J. & Diagana, T. T. Cryptosporidiosis drug discovery: opportunities and challenges. *ACS Infect. Dis.* **2,** 530–537 (2016).
20. Branchini, B. R. *et al.* Red-emitting luciferases for bioluminescence reporter and imaging applications. *Anal. Biochem.* **396,** 290–297 (2010).
21. Theodos, C. M., Griffiths, J. K., D'Onfro, J., Fairfield, A. & Tzipori, S. Efficacy of nitazoxanide against *Cryptosporidium parvum* in cell culture and in animal models. *Antimicrob. Agents Chemother.* **42,** 1959–1965 (1998).
22. Zambriski, J. A. *et al.* Description of fecal shedding of *Cryptosporidium parvum* oocysts in experimentally challenged dairy calves. *Parasitol. Res.* **112,** 1247–1254 (2013).
23. Zambriski, J. A. *et al. Cryptosporidium parvum*: determination of ID_{50} and the dose-response relationship in experimentally challenged dairy calves. *Vet. Parasitol.* **197,** 104–112 (2013).
24. Bellosa, M. L. *et al.* A comparison of fecal percent dry matter and number of *Cryptosporidium parvum* oocysts shed to observational fecal consistency scoring in dairy calves. *J. Parasitol.* **97,** 349–351 (2011).

Supplementary Information is available in the online version of the paper.

Acknowledgements We thank S. Tzipori and D. Girouard for *C. hominis* oocysts; B. Nare for screening; B. H. Lee and J. Selva for high-content imaging data; M. Weaver for rat toxicology studies; I. Mueller for monkey pharmacokinetics; B. Yeung, O. Simon, J. Roland, V. Bollu, A. Chatterjee, A. Nagle, R. Moreau, and P. K. Mishra for compound synthesis; other Novartis Institutes for Biomedical Research (NIBR) colleagues for profiling; J. Burrows and K. Chibale for MMV390048; and M. Meissner for a plasmid carrying the red-shifted Fluc gene. This work was supported in part by the NIBR, the Wellcome Trust (Pathfinder 107678/Z/15/Z to B.S. and U.H.M.), and the National Institutes of Health (NIH R01AI112427 to B.S.). Inhibitors of the *Plasmodium* PI4K were discovered with the support of translational grants (WT078285 and WT096157) from the Wellcome Trust and funding from the Medicines for Malaria Venture (M.M.V.). B.S. is a Georgia Research Alliance Distinguished Investigator and A.S. is supported by NIH Fellowship F32AI124518. We thank our colleagues from Novartis Institute for Tropical Diseases, University of Georgia, Athens, Washington State University's Office of the Campus Veterinarian, Animal Resource Unit, and the Office of Research Support and Operations and R. Anderson, 5D Dairy Farm, for their support. We are also grateful to the animal science and veterinary students at Washington State University for their participation in data collection and care of the research calves.

Author Contributions U.H.M., S.V., J.A.Z., B.S., and T.T.D. conceived and designed the study; B.S. wrote grant applications with contributions from U.H.M.; U.H.M., A.T.C., and G.M.C.B. developed *C. parvum* screening assays; C.G.N. and S.H.L. developed enzyme assays; C.B. analysed *P. falciparum* EC_{50} data; U.H.M., P.G., and T.T.D. assembled the screening library; R.R.K. and B.Z. performed compound synthesis; U.H.M., B.Z., and J.W. analysed the structure–activity relationship; S.B.L. and F.B. analysed *in vivo* pharmacokinetics data; L.Z. optimized formulation; U.H.M., G.F., F.J.L., and T.T.D. analysed *in vivo* efficacy and toxicology results; S.V., A.S., and B.S. designed mouse models based on transgenic parasites; S.V., A.S., and J.T. constructed transgenic parasites; S.V., A.S., C.F.B. and G.T.H. validated mouse models; G.T.H., S.V., and C.F.B. tested compounds; J.A.Z. developed the calf model and analysed calf data; T.L.S. executed the calf model; S.N. conducted anatomic pathology reviews for efficacy and toxicity; L.B.G. developed and executed calf stool analytics; and B.S., S.V., U.H.M., and T.T.D. wrote the manuscript with contributions from J.A.Z., A.T.C., C.G.N., and S.B.L.

Author Information Reprints and permissions information is available at www.nature.com/reprints. The authors declare competing financial interests: details are available in the online version of the paper. Readers are welcome to comment on the online version of the paper. Publisher's note: Springer Nature remains neutral with regard to jurisdictional claims in published maps and institutional affiliations. Correspondence and requests for materials should be addressed to T.T.D. (thierry.diagana@novartis.com), B.S. (striepen@uga.edu), or J.A.Z. (jzambriski@vetmed.wsu.edu).

Reviewer Information *Nature* thanks J. S. Doggett, N. S. Gray and the other anonymous reviewer(s) for their contribution to the peer review of this work.

© 2017 Macmillan Publishers Limited, part of Springer Nature. All rights reserved.

METHODS

Compounds. KDU691, BQR695, and MMV390048 were synthesized as described earlier[12,25]. Synthesis of KDU731 and other pyrazolopyridine analogues is described in the Supplementary Information and in a patent application[14].

Cells and parasites. Human ileocecal adenocarcinoma cells (HCT-8) were purchased from American Type Culture Collection (ATCC; CCL-34), tested for mycoplasma (at Novartis Institute for Tropical Diseases, not at University of Georgia, Athens), and maintained in RPMI-1640 medium supplemented with 10% heat-inactivated horse serum. *C. parvum* and *C. hominis* oocysts were purchased from the Sterling Laboratory, University of Arizona, and Tufts University Cummings School of Veterinary Medicine. Oocysts were used in infection experiments less than 3 months after the date of shedding. Excystation and infection protocols followed established methods with modifications[26]. Oocysts were treated with 10 mM hydrochloric acid (HCl) in 1× Hank's balanced salt solution (HBSS) for 10 min with agitation at 37 °C, then washed twice with non-acidic 1× HBSS. Oocysts were excysted at a density of 10^6 primed oocysts per microlitre in parasite infection medium (1:1 Leibovitz's L-15 medium and UltraCULTURE medium supplemented with 2 mM sodium taurocholate, 10% heat-inactivated horse serum, and 200 μM L-ascorbic acid). All dilutions for subsequent assays were performed in parasite infection medium without sodium taurocholate.

High-content imaging immunofluorescence *Cryptosporidium* screening assay. A previously reported *C. parvum* high-content imaging assay in HCT-8 cells was used with modifications[27,28] and is described in detail in the Supplementary Information.

***Cryptosporidium* EC_{50} determination.** High-content imaging HCT-8 cell infection assays with *C. parvum* and *C. hominis* were conducted following established protocols[27] in 384-well flat, black clear-bottom plates using an Opera QEHS (PerkinElmer) imaging system. We also developed a cytopathic effect (CPE)-based assay monitoring host cell viability using CTG reagent (Promega) that did not require staining or imaging. Further details on EC_{50} determination for *C. parvum* and *C. hominis* using both assays in a ten-point dose–response with threefold compound dilution will be described elsewhere (A.T.C. *et al.*, manuscript in preparation). The EC_{50} of KDU731 was also determined using Nluc-expressing parasites[8]. In brief, HCT-8 cells were infected with purified Nluc-expressing parasites (1,000 oocysts per well) and incubated with different concentrations of KDU731 for 48 h. Culture supernatant was removed from the wells and 200 μl of Nano-Glo lysis buffer containing 1:50 of Nano-Glo substrate (Promega) was added to the wells. Lysate was transferred to 96-well plates and luminescence was measured on a Synergy H4 Hybrid Microplate Reader (BioTek Instruments).

Host cell cytotoxicity assay. Cytotoxicity against HepG2 ATCC CRL-10741 was determined as previously described[29]. Cells were seeded into 384-well plates at 400 cells per well, incubated at 37 °C for 24 h and exposed to threefold serially diluted compounds for 96 h. Cell viability was monitored using a Cell Counting Kit-8.

Baculovirus expression and purification of *C. parvum* PI(4)K. The full-length coding sequence of *C. parvum* PI(4)K (cgd8_4500) was codon-optimized for baculovirus expression, synthesized, and cloned into pFastBac-HTb (Invitrogen) in frame with an amino (N)-terminal polyhistidine tag using the BamHI and HindIII restriction sites. Recombinant pFastBacHTb-CpPI(4)K bacmid clones were generated by site-specific transposition in *Escherichia coli* DH10Bac (Invitrogen). The bacmid sequence was confirmed by direct DNA sequencing. Bacmid isolation, transfection, and selection of the recombinant viruses was performed according to the manufacturer's protocol (Bac-to-Bac System, Invitrogen). SF9 cells, cultured in SF-900 III serum-free medium, were transfected with recombinant baculovirus at 1/200 (v/v) and incubated at 27 °C for 72 h. Pellets were collected after centrifugation and re-suspended in cell lysis buffer (20 mM Tris-HCl, pH 7.5, 300 mM NaCl, 1 mM DTT, 20 mM imidazole, 0.01% Triton X-100 and 1× complete protease inhibitor cocktail without EDTA (Roche Diagnostics)). The cell suspension was lysed by sonication and clarified supernatant was loaded onto a 1 ml HisTrap affinity column (GE Healthcare) pre-equilibrated with buffer A (20 mM Tris-HCl, pH 7.5, 300 mM NaCl, 1 mM DTT, 20 mM imidazole, and 1× complete protease inhibitor cocktail without EDTA). The column was washed with buffer A containing 45 mM imidazole and the bound protein was eluted with buffer A with 90 mM imidazole. Fractions containing CpPI(4)K were pooled, concentrated using Amicon Ultra-15, and purified by a gel-filtration column (Hi-Load 26/60 Superdex 200, GE Healthcare), equilibrated with 20 mM Tris, pH 7.5, 300 mM NaCl, 1 mM DTT and 1× protease inhibitor cocktail without EDTA. Aliquots were flash frozen in liquid nitrogen and immediately stored at −80 °C. Mutations (CpPI4K-S871L and CpPI4K- H1037Y) were introduced into CpPI(4)K in the pFastBac plasmid using a QuikChange Site-Directed Mutagenesis Kit (Agilent) and confirmed by DNA sequencing. Mutant proteins were expressed, purified, and assayed as described for the wild-type protein and did not show significant change in their KDU731 IC_{50} (see Supplementary Information for full details).

PI(4)K enzymatic assay. The CpPI(4)K enzyme assay was described earlier[12]. Briefly, L-α-phosphatidylinositol (Avanti Polar Lipids), dissolved in 3% *n*-octylglucoside (Roche Diagnostics), was used as lipid substrate using a Transcreener ADP_2 FP detection kit (BellBrook Labs) in black, solid 384-well plates (Corning 3575). The final assay volume was 10 μl and contained 3 nM CpPI(4)K in 10 mM Tris, pH 7.5, 1 mM DTT, 3 μM ATP, 5 mM Mn^{2+}, 0.05% Triton X-100, and 10 μM phosphatidylinositol/octylglucoside. The enzyme reaction was performed for 50 min at room temperature and stopped by adding 10 μl of detection mix containing 50 mM HEPES, pH 7.5, 400 mM NaCl, 20 mM EDTA, and 0.02% Brij-35, 2 nM AMP Alexa Fluor 633 tracer, and 20 μg ml^{-1} ADP antibody (BellBrook Labs). Fluorescence polarization measurements were performed on an Infinite M1000 plate reader (Tecan) with excitation and emission wavelengths of $\lambda_{ex} = 635$ nm and $\lambda_{em} = 680$ nm (20-nm bandwidth). IC_{50} values were calculated using GraphPad Prism software.

Solubility, permeability, *in vitro* metabolic stability, and *in vitro* safety assessment. Solubility was measured using a miniaturized shake-flask approach and streamlined high-performance liquid chromatography (HPLC) analysis as described earlier[30]. Parallel artificial membrane assays were performed using a standard protocol[31]. The metabolic stability in liver microsomes was determined using the compound depletion approach and quantified by liquid chromatography/mass spectrometry (LC/MS). The assay measures the rate and extent of metabolism as determined by the disappearance of the parent compound, which allows the determination of *in vitro* half-life ($t_{1/2}$), intrinsic clearance, and the prediction of metabolic clearance in various species[30]. Cardiotoxicity and mini-ames genotoxicity[32] risk was measured as previously described[30]. All assays for binding to proteins known to bear potential safety liabilities in humans were high-throughput competitive binding assays using specific radiolabelled ligands[30]. The phototoxicity assay was performed following OECD Guidelines for Testing of Chemicals 432 (*in vitro* 3T3 NRU phototoxicity test).

Cytochrome P450 analysis. KDU731 was subjected to CYP450 inhibition analysis using three different isoforms[30]. The compounds were assessed for time-dependent inhibition using CYP3A4 (ref. 30). The CYP induction assay was performed using a PXR receptor; binding was assayed using a LanthaScreen TR-FRET PXR (SXR) competitive binding assay kit from Invitrogen[30].

***In vivo* pharmacokinetic analysis.** Rodent *in vivo* pharmacokinetic analysis was conducted using non-randomized CD-1 female mice ($n = 4$, 6–8 weeks old) and Wister rats ($n = 4$, 6–8 weeks old). Pharmacokinetic studies in monkeys ($n = 3$) were performed in rhesus macaques as described[16]. Neonatal calf pharmacokinetic studies were performed as part of the efficacy study on day 1 and day 7 of treatment. All procedures involving animals were reviewed and approved by the respective institutional animal care and use committees. No statistical methods were used to predetermine sample size. Sample size was determined on the basis of the minimum number of animals required for good data distribution and statistics. Blinding was not possible in these experiments but animals were selected randomly for each group. KDU731 was formulated in suspension formulation for per os dosing and solution formulation for intravenous dosing as described in Extended Data Table 3. For rat toxicology studies, KDU731 was formulated in solid dispersion. KDU731 (20%) and the required excipients (37.5% Soluplus, 37.5% Eudragit E PO, and 5% SLS) were dissolved in ethanol/dichloromethane (v/v = 1:1) at a total solid concentration of 10 g l^{-1} by sonication and heating to 50 °C. The solution was spray dried using a Buchi B290 Mini spray dryer with an inlet temperature of 75 °C, aspirator set to 100%, and pump to 35%, followed by overnight drying under vacuum at 40 °C. The amorphous nature was confirmed by X-ray powder diffraction analysis and powder was stored at 4 °C. Solid dispersion powder suspension was prepared freshly in 0.5% HPMC in 50 mM acetate buffer (pH 4.7) at 10 mg ml^{-1} of KDU731 (equivalent to solid dispersion powder 50 mg ml^{-1}) and rats were dosed within 1 h of preparation. Blood samples for pharmacokinetic studies were collected between 0 and 24 h post-dose. Compound plasma concentrations were determined by LC/MS. Plasma samples from pharmacokinetic studies were extracted with acetonitrile:methanol:acetic acid (90:9.8:0.2) containing warfarin as an internal standard, using an 8.8:1 extractant to plasma ratio. Analyte quantitation was performed by LC/MS/MS. Liquid chromatography was performed using an Agilent 1200 HPLC system, with an Agilent Zorbax Phenyl (3.5 μm, 4.6 mm × 75 mm) column at an oven temperature of 45 °C, coupled with a API4000 triple quadruple mass spectrometer (Applied Biosystems). Pharmacokinetic parameters were determined using Watson LIMS software, by non-compartmental analysis.

Rat toxicology study. KDU731 solid dispersion powder suspension was prepared freshly in 0.5% HPMC in 50 mM acetate buffer (pH 4.7) at 10 mg ml^{-1} and was orally administered to five male Wistar rats at a daily oral dose of 30 or 100 mg per kg (body weight) per day for 2 weeks. Five control animals were treated with vehicle only. Rats were obtained from Shanghai SLAC Animal and subjected to

© 2017 Macmillan Publishers Limited, part of Springer Nature. All rights reserved.

3 days of quarantine and acclimatization before study begin. All animals were subjected to daily clinical observation, and body weight and food consumption were determined for all animals enrolled in the study. Clinical laboratory evaluations (haematology and clinical chemistry) were performed at the scheduled necropsy on day 15. Organs were examined for gross pathology and weighed before fixation and preparation for histology. Samples from organs and tissues prepared from animals assigned to control and high-dose groups were examined microscopically. Specifically, the heart, pancreas, gastrointestinal tract (oesophagus, stomach, duodenum, jejunum, ileum, caecum, colon, rectum), kidney, liver, spleen, lung, testes, epididymis, adrenals, and thymus were examined for histopathological changes.

Engineering of a *C. parvum* transgenic parasite strain expressing red-shifted Fluc. The 5′ untranslated region (UTR) and 3′ UTR of the *C. parvum* actin gene were amplified from parasite genomic DNA and ligated into the KpnI/ClaI and SpeI/BamHI sites of plasmid TK-Eno-Nluc-Neo-TK[8], respectively. The coding sequence for red-shifted luciferase[20] was amplified from pTubRE9 vector (a gift from M. Meissner, University of Glasgow, UK) and cloned into SalI/NheI restriction sites replacing Nluc. A 404-base-pair fragment of the 5′ TK flank, the *tk* gene, and a ribosomal 3′ UTR were inserted upstream of the 5′ actin UTR using Gibson Assembly cloning (New England Biolabs). The final vector, along with the Cas9 plasmid containing a TK guide RNA (GAAGAATACAATTTCTAAGG) targeting the 3′ end of the *tk* gene, was used to transfect *C. parvum* sporozoites. Sporozoites were delivered by surgery into the small intestine of C57BL/6 IFN-γ knockout mice (B6.129S7-Ifngtm1Ts/J, Jackson Laboratory) using procedures described previously[8]. Note that UGA1 Nluc parasites were generated using *C. parvum* IOWA II oocysts purchased from Sterling Parasitology Laboratory, University of Arizona, whereas the UGA2 Fluc strain was engineered using *C. parvum* IOWA II oocysts purchased from Bunch Grass Farms, Deary, Idaho, USA.

Mouse model following faecal oocyst load. All mouse studies described in this section were approved by the Institutional Animal Care and Use Committee of the University of Georgia (animal use protocol number A2016 01-028-Y1-A4). C57BL/6 IFN-γ knockout mice aged 6–8 weeks were selected randomly for each group ($n = 5$) and infected with 10,000 *C. parvum* UGA1 Nluc[8] oocysts. No statistical tests were used to predetermine sample size. KDU731 was formulated in 0.5% (w/v) methylcellulose and 0.5% (w/v) polysorbate in water and administered to mice daily for 7 days by oral gavage beginning on day 3 or day 11 after infection. Control mice were given only vehicle. Mice were monitored for weight loss, fur ruffling, hunched posture, and inactivity. Mice showing a weight loss of equal to or greater than 15% were euthanized. Faecal samples were collected (not blinded) and luminescence measurements were performed as described[8] (parasite Nluc activity is stable in faeces when refrigerated). Measurements were performed on faeces collected from individual mice as well as from cage-wide (pooled) collections. For Nluc assay, 20 mg of faeces was mashed in 1 ml of lysis buffer (50 mM Tris-HCl (pH 7.6), 2 mM DTT, 2 mM EDTA, 10% glycerol, 1% Triton X-100), ten 3-mm glass beads were added to the tube, followed by vigorous agitation using a vortex mixer for 1 min and a short spin to pellet faecal material. Three aliquots of 100 µl lysate were dispensed into 96-well white plates and an equal amount of Nano-Glo reconstituted buffer containing 1:50 of Nano-Glo substrate (Promega) was added, luminescence was read using a Synergy H4 Hybrid Microplate Reader (BioTek Instruments).

To measure oocyst load by qPCR, DNA was isolated from 100 mg of faeces. Samples were subjected to five rounds of freezing in liquid nitrogen and thawing in 100 °C heater block before DNA isolation using a ZR Faecal DNA Miniprep Kit (Zymo Research, Irvine, California, USA). qPCR was performed using sample DNA along with standards prepared from uninfected faeces spiked with oocysts. PCR primers JVAF and JAVR and probe 5′ FAM-labelled JVAR[33] were used along with the following cycling parameters: denaturation at 95 °C for 3 min, followed by 40 cycles of denaturation at 95 °C for 10 s, and annealing at 60 °C for 30 s. Each 20 µl PCR reaction contained 10 µl of SSoAdvanced Universal Probes Supermix (Bio-Rad Laboratories, Hercules, California, USA), 0.4375 µM of each primer, 0.125 µM probe, and 2 µl DNA.

Mouse model following tissue parasite load using whole-animal imaging. IFN-γ knockout mice ($n = 5$ per group) were infected with 10,000 *C. parvum* UGA2 Fluc oocysts expressing red-shifted Fluc and given a daily dose of 10 mg per kg (body weight) KDU731, nitazoxanide (Sigma) at 100 mg per kg (body weight), or control formulation for one week by oral gavage starting on day 7 after infection. Parasite tissue load was measured by *in vivo* imaging. At the beginning of the experiment, the abdominal area of mice was shaved with clippers to increase the signal during imaging on an IVIS Lumina II system (Caliper Life Sciences). Mice were injected subcutaneously with 125 mg per kg (body weight) D-luciferin (Gold Biotechnology, St Louis, Missouri, USA). Five minutes after luciferin injection, mice were anaesthetized in an induction chamber using 3% isofluorane and then placed in the camera chamber. Mice were kept under anaesthesia by administering isofluorane through individual nose cones. Images were acquired using a setting of *F*-stop = 1/16, binning = medium, and an exposure time of 5 min. Regions of interest were selected for each mouse and total flux (photons per second) was quantified using IVIS Lumina II Living Image 4.0 Software (Caliper Life Sciences). To validate measurements of parasite tissue burden, mice infected for 1 week were imaged, killed, and the small intestine was removed and cut into 12 (1-cm) segments, and flushed with PBS. Sections were imaged three times in PBS with D-luciferin, after which genomic DNA was isolated from each segment using a ZR Faecal DNA Miniprep Kit (Zymo Research, Irvine, California, USA). qPCR was performed using the parameters described above and parasite burden was established against a standard curve of samples with known parasite DNA content.

Histology of intestinal tissue. Mice treated with KDU731 or control formulation were killed and intestinal tissue was collected within 15 min of death. Sections of the small intestine were taken from the 1–2 cm region anterior to the caecum, flushed with PBS, and fixed overnight in 10% buffered formalin. Fixed samples were embedded in paraffin and 4 µm sections were cut (RM225 Microtome, Leica, Buffalo Grove, Illinois, USA). Sections were de-paraffinized and stained with haematoxylin and eosin.

Neonatal calf efficacy study. All calves used in this study were cared for in compliance with the Washington State University Institutional Animal Care and Use Committee. Sample size was calculated assuming that 85% of treated calves had resolution of clinical illness by the end of the treatment period (48 h after administration of treatment number 14) compared with 15% of control calves. Assuming a type I error risk of 5% and a type II error risk of 80%, seven calves were needed in the treatment group, plus two positive controls. In the event of calf death or removal from the study, an additional four calves were added to the control group ($n = 6$). Sample size was calculated using Epi Info. Fifteen Friesian–Holstein bull calves were enrolled in November 2015 and February 2016. At birth, all calves enrolled in November were randomized to treatment with KDU731 ($n = 7$), positive infection control ($n = 2$), and negative infection control ($n = 1$). The five calves enrolled in February were positive controls. The perineum of the dam was cleaned with povidone–iodine scrub, and calves were delivered onto single-use plastic sheets to prevent exposure to environmental pathogens. Calves with abnormal physical examination findings and those weighing less than 29.5 kg at birth were excluded. Enrolled calves received 4 l ≥ 50 g IgG/l commercial colostrum replacer (Land O'Lakes) and a 3 ml subcutaneous injection of vitamin E and selenium (Merck Animal Health). Calves were then transported from the commercial dairy farm to Washington State University where they were housed in individual box stalls in a BSL-2 facility. Shatter-proof mirrors were provided for enrichment. Within 48 h of birth, blood samples were collected and evaluated for adequate passive transfer of colostral immunity. Calves were offered a commercial 20% protein/20% fat non-medicated milk replacer (Land O'Lakes) every 12 h via nipple bucket. At each feeding, calves were fed an average of 8.8 g of dry matter per kilogram of birth weight for the duration of the study. Water was provided *ad libitum*. All calves randomized to treatment or positive control groups were experimentally challenged within the first 48 h of life with 5×10^7 *C. parvum* oocysts (Iowa II, Bunch Grass Farm, ID) through the rigid portion of an oroesophageal feeding tube. Oocysts were within 1 month of isolation and were cleaned in 0.6% sodium hypochlorite for 1 min and then washed four times with PBS. The negative control calf was sham-challenged to maintain blinding of study personnel.

To facilitate collection of blood for plasma pharmacokinetic analysis, a long-term intravenous catheter (MILACATH, MILA International) was aseptically placed in the jugular vein within the first 48–72 h of life. Calves were sedated with 0.1 ml intravenous xylazine (20 mg ml^{-1}) (Akorn Animal Health). Sedation was reversed with 0.1 ml intramuscular atipamezole (5 mg ml^{-1}) (Zoetis). Beginning at birth, a faecal sample was collected directly from the rectum every 24 h. A complete physical examination was performed every 12 h, and clinical data including appetite, mentation, faecal consistency, and hydration status were recorded. Clinical data were evaluated on a scale of 1 (normal) to 3 (severe) in accordance with previously described methods (see rubric in Supplementary Information)[23,24].

KDU731 was prepared as a 5 mg ml^{-1} suspension formulation in 0.5% (w/v) methylcellulose and 0.5% w/v Tween-80 in water, and KDU731 treatment was initiated when a calf began shedding oocysts and had a faecal consistency score of 3. Calves were induced to suckle and then KDU731 was given orally via an oral dosing syringe. Calves were treated every 12 h for 7 days at a dose of 5 mg per kg birth-weight at least 2 h after feeding. Pharmacokinetic sampling was conducted on day 1 and day 7 of treatment. Blood was drawn before and at multiple time-points after administration. A faecal sample was collected 1 h and 12 h after administration. On days 2–6 of treatment, blood was collected before KDU731 administration. On day 3 of life, a faecal sample was tested for *E. coli* K99, and on day 7 for *Salmonella*, rotavirus, and corona virus. Of the seven treatment calves, two (N101 and N107) were randomly selected to be euthanized 24 h after administration of the final KDU731 treatment. A positive control calf (N104) was also euthanized at the same

© 2017 Macmillan Publishers Limited, part of Springer Nature. All rights reserved.

time. Euthanasia was by captive bolt and induction of bilateral pneumothorax to avoid confounding histological findings. Calves were submitted for necropsy to the Washington State Animal Disease Diagnostic Laboratory. Samples of the liver, spleen, kidney, and small intestine were collected for histological analysis. The remaining calves continued in the study until the cessation of faecal oocyst shedding as determined by immunofluorescence microscopy (Merifluor, Meridian Diagnostics). Upon cessation of faecal oocyst shedding (two consecutive negative faecal samples over 48 h), calves were euthanized and submitted to the Washington State Animal Disease Diagnostic Laboratory for necropsy.

Oocysts counts were interpolated by qPCR at the Cornell Animal Health Diagnostic Center using serial dilutions of commercially purified *C. parvum* oocysts (Waterborne, New Orleans, Louisiana, USA). Total nucleic acid was extracted from supernatants of 200 mg of faecal sample, oocyst suspension, or negative control homogenized in 400 µl of PBS using a magnetic-bead-based automated procedure (AM1840, Applied Biosytems, Foster City, California, USA). An exogenous control (MS2 phage) was added to the lysis buffer to control for PCR inhibition[34]. qPCR for *Cryptosporidium* spp. 18S rRNA was performed on an Applied Biosystems 7500-FAST platform using commercial master mix (ToughMix, Quantabio) and oligonucleotides previously described[35]. This count was standardized by the faecal dry weight percentage. A 5–10 g portion of each original faecal sample was dried at 108 °C for a minimum of 24 h (Squaroid Vaccuum Oven, Labline, India) and weighed[24].

Data were analysed using descriptive and inferential methods. A Shapiro–Wilk test was used to determine whether data were non-Gaussian. Depending on the distribution of data, continuous variables were evaluated using a Student's *t*-test, analysis of variance, or a Wilcoxon rank-sum test. Analysis of variance was used to assess differences in faecal oocyst counts and faecal consistency score between the KDU731-treated and untreated calves. The effect of comorbidity on outcomes of interest was evaluated using a Student's *t*-test. Data were analysed using JMP Pro 11.0 (SAS Institute).

Data availability. Source data analysed for mouse and calf infection experiments shown in Figs 2 and 3 are included as Microsoft Excel files in the Supplementary Information. Requests for compounds (Novartis Institute for Tropical Diseases) and transgenic parasite strains (University of Georgia, Athens) are subject to a Material Transfer Agreement. All other data are available from the corresponding authors upon reasonable request.

25. Younis, Y. *et al.* 3,5-Diaryl-2-aminopyridines as a novel class of orally active antimalarials demonstrating single dose cure in mice and clinical candidate potential. *J. Med. Chem.* **55,** 3479–3487 (2012).
26. Castellanos-Gonzalez, A. *et al. Cryptosporidium* infection of human intestinal epithelial cells increases expression of osteoprotegerin: a novel mechanism for evasion of host defenses. *J. Infect. Dis.* **197,** 916–923 (2008).
27. Bessoff, K., Sateriale, A., Lee, K. K. & Huston, C. D. Drug repurposing screen reveals FDA-approved inhibitors of human HMG-CoA reductase and isoprenoid synthesis that block *Cryptosporidium parvum* growth. *Antimicrob. Agents Chemother.* **57,** 1804–1814 (2013).
28. Sharling, L. *et al.* A screening pipeline for antiparasitic agents targeting cryptosporidium inosine monophosphate dehydrogenase. *PLoS Negl. Trop. Dis.* **4,** e794 (2010).
29. Manjunatha, U. H. *et al.* Direct inhibitors of InhA are active against *Mycobacterium tuberculosis*. *Sci. Transl. Med.* **7,** 269ra3 (2015).
30. Faller, B. *et al.* High-throughput *in vitro* profiling assays: lessons learnt from experiences at Novartis. *Expert Opin. Drug Metab. Toxicol.* **2,** 823–833 (2006).
31. Faller, B. Artificial membrane assays to assess permeability. *Curr. Drug Metab.* **9,** 886–892 (2008).
32. Ames, B. N., Lee, F. D. & Durston, W. E. An improved bacterial test system for the detection and classification of mutagens and carcinogens. *Proc. Natl Acad. Sci. USA* **70,** 782–786 (1973).
33. Jothikumar, N., da Silva, A. J., Moura, I., Qvarnstrom, Y. & Hill, V. R. Detection and differentiation of *Cryptosporidium hominis* and *Cryptosporidium parvum* by dual TaqMan assays. *J. Med. Microbiol.* **57,** 1099–1105 (2008).
34. Dreier, J., Störmer, M. & Kleesiek, K. Use of bacteriophage MS2 as an internal control in viral reverse transcription-PCR assays. *J. Clin. Microbiol.* **43,** 4551–4557 (2005).
35. Operario, D. J., Bristol, L. S., Liotta, J., Nydam, D. V. & Houpt, E. R. Correlation between diarrhea severity and oocyst count via quantitative PCR or fluorescence microscopy in experimental cryptosporidiosis in calves. *Am. J. Trop. Med. Hyg.* **92,** 45–49 (2015).

© 2017 Macmillan Publishers Limited, part of Springer Nature. All rights reserved.

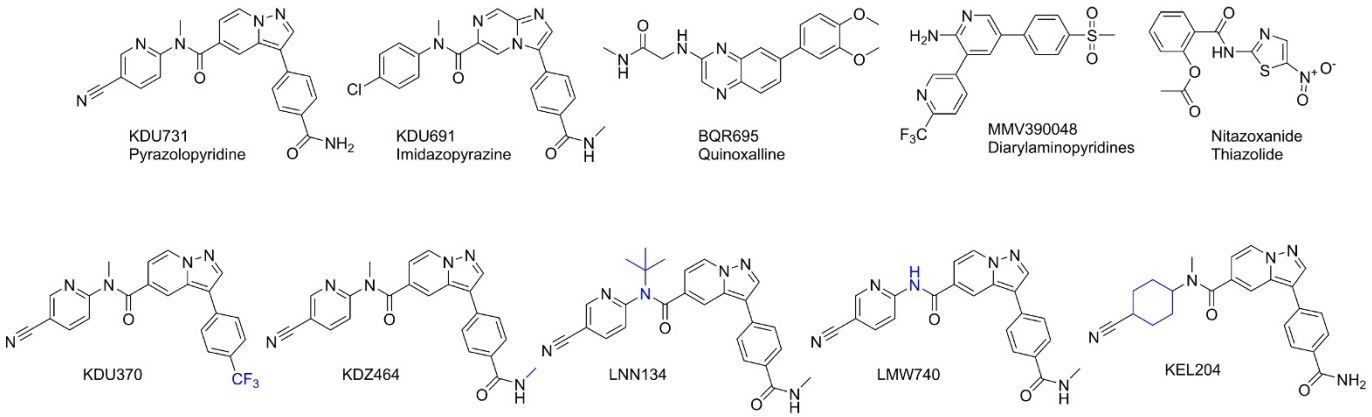

Extended Data Figure 1 | Structures of the pyrazolopyridines and other known PI(4) kinase inhibitors. Compounds described in Table 1. Important structural determinants required for anti-*Cryptosporidium* activity in pyrazolopyridines are shown in blue.

© 2017 Macmillan Publishers Limited, part of Springer Nature. All rights reserved.

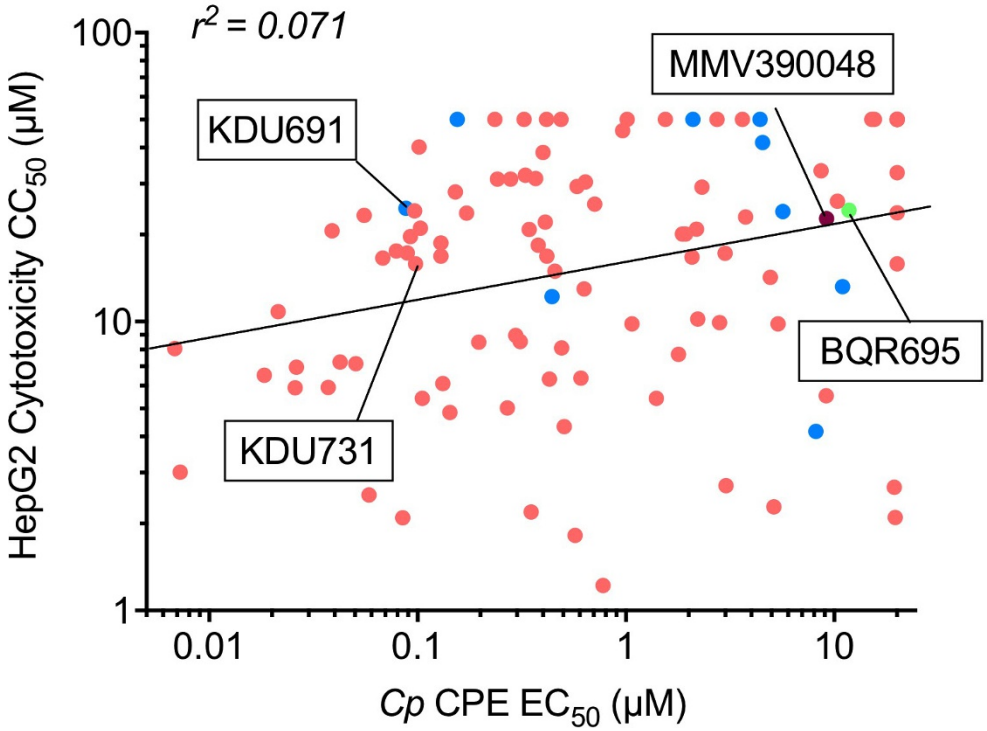

Extended Data Figure 2 | Anti-*Cryptosporidium* activity does not correlate with mammalian cell toxicity. Correlation of *C. parvum* cytopathic effect versus HepG2 cytotoxicity assay for selected pyrazolopyridine and imidazopyrazine analogues along with BQR695 and MMV390048. Data shown here are geometric mean EC_{50} values, with at least two biological replicates.

© 2017 Macmillan Publishers Limited, part of Springer Nature. All rights reserved.

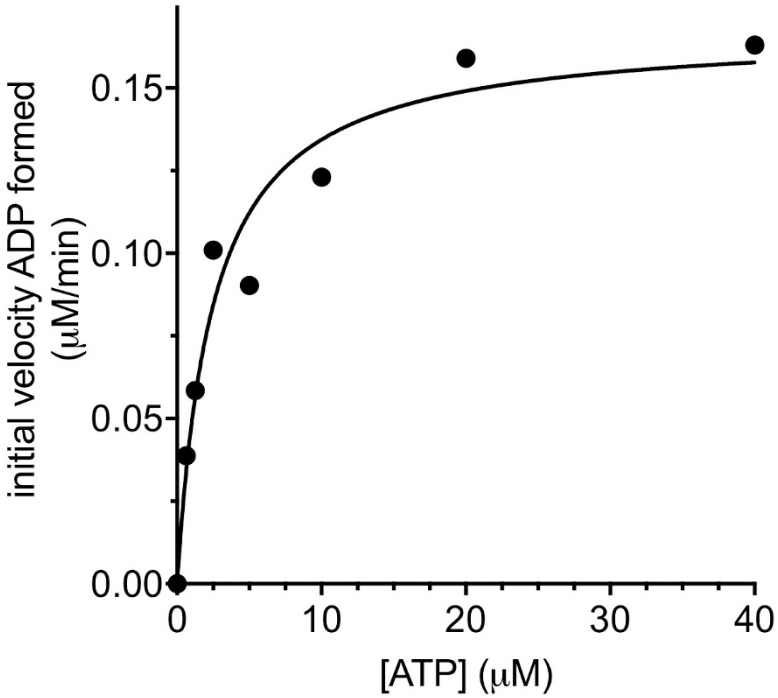

Extended Data Figure 3 | Recombinant *C. parvum* cgd8_4500 shows phosphatidylinositide kinase activity. *C. parvum* cgd8_4500 was expressed in insect cells using a Baculovirus system and recombinant enzyme was purified. A Michaelis–Menten plot of phosphatidylinositide kinase reaction with 3 nM CpPI(4)K enzyme at varying ATP concentrations is shown. Data shown here are a representative graph of two independent biological replicates.

© 2017 Macmillan Publishers Limited, part of Springer Nature. All rights reserved.

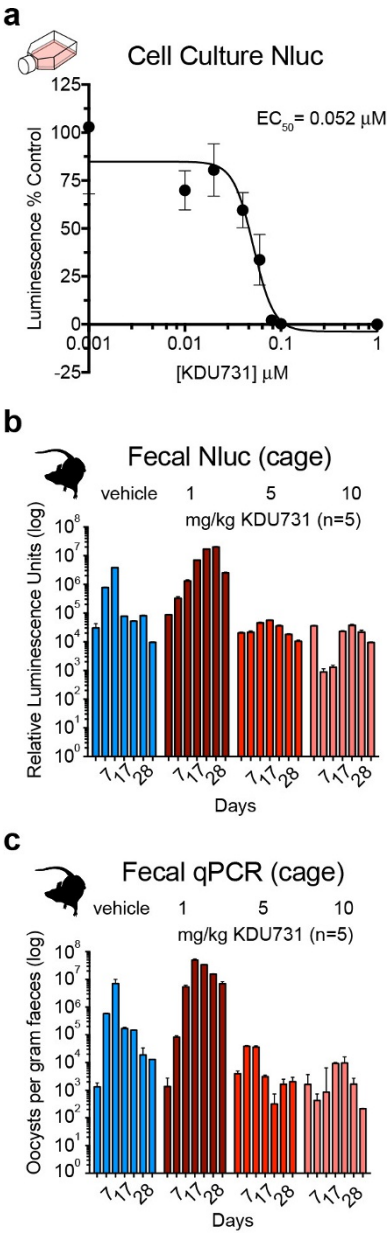

Extended Data Figure 4 | KDU731 inhibits *C. parvum* Nluc parasites *in vitro* and *in vivo*. **a**, EC_{50} determination of KDU731 against UGA1 Nluc transgenic parasites grown in HCT-8 cultures using luciferase activity as read out. Representative data are shown, three technical replicates. **b**, Mice ($n = 5$) were infected with 10,000 UGA1 Nluc oocysts and treated orally 3 days after infection with 1, 5, or 10 mg per kg (body weight) KDU731 for 1 week. Faecal oocyst load was determined by measuring parasite luciferase activity (**b**) or parasite DNA by qPCR (**c**) in faeces pooled from entire cage of five mice (20 mg faeces for Nluc and 100 mg for PCR assay). **b**, **c**, Means for three technical replicates are shown. Error bars, s.d. Pooled Nluc experiments for vehicle and 10 mg per kg (body weight) dose were repeated in three biological replicates and a representative result is shown.

© 2017 Macmillan Publishers Limited, part of Springer Nature. All rights reserved.

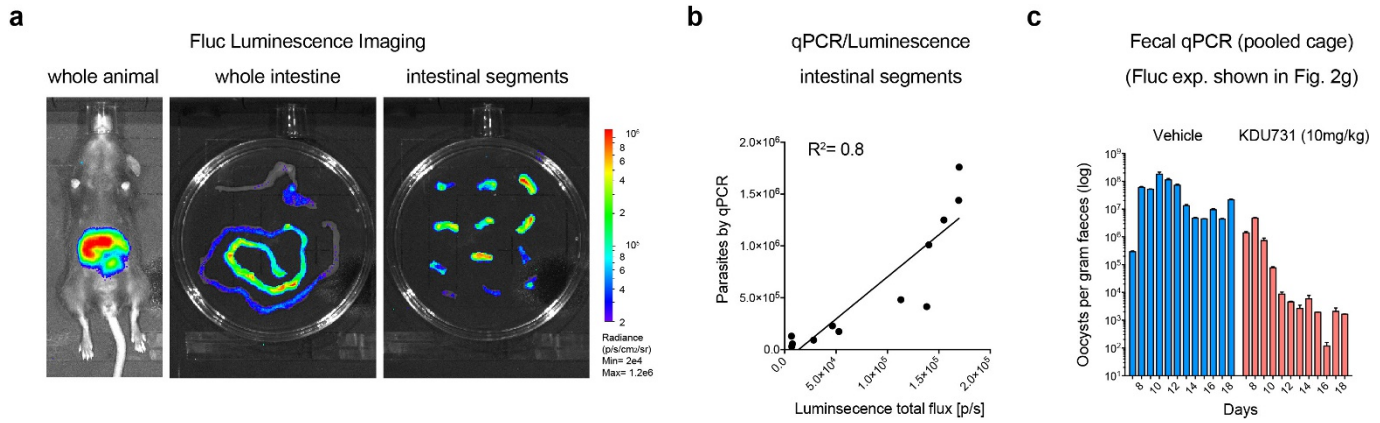

Extended Data Figure 5 | Parasite intestinal load measured by qPCR correlates with faecal shedding and tissue luminescence. a, Mice ($n = 4$) were infected with 50,000 UGA2 FLuc oocysts and imaged after 1 week. Mice were killed and the small intestine was resected and imaged (representative image shown). Infection of the intestine ranged in intensity from heavy in the ileum to more moderate in the jejunum and caecum (see radiance scale bar for comparison). Intestines were cut into 12 segments and the luminescence of each segment was recorded. **b**, qPCR analysis of intestinal segments was performed in triplicate and plotted against the respective luminescence measurements. Regression analysis found robust correlation of tissue luminescence and PCR for parasite DNA, with $r^2 = 0.8$. **c**, Mice were infected with 10,000 UGA2 FLuc oocysts, and 7 days after infection animals were treated daily for a week with vehicle or 10 mg per kg (body weight) KDU731. Whole-animal imaging during the treatment period is shown in Fig. 2g. Faecal oocyst load was determined by measuring parasite DNA by qPCR in faeces pooled from a cage of five mice. Error bars, s.d.

© 2017 Macmillan Publishers Limited, part of Springer Nature. All rights reserved.

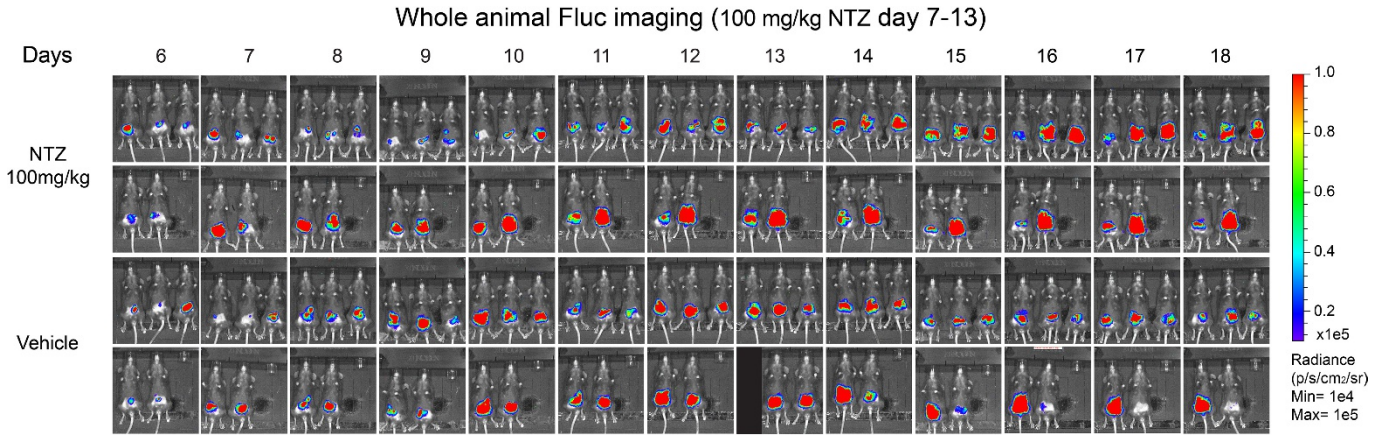

Extended Data Figure 6 | Nitazoxanide does not reduce intestinal parasite load in IFN-γ knockout mice. Mice ($n = 5$) were infected with 10,000 UGA2 FLuc oocysts, and 7 days after infection animals were treated daily for a week with 100 mg per kg (body weight) nitazoxanide or vehicle. Mice were monitored by whole-animal imaging. Radiance scale shows total flux in photons per second.

© 2017 Macmillan Publishers Limited, part of Springer Nature. All rights reserved.

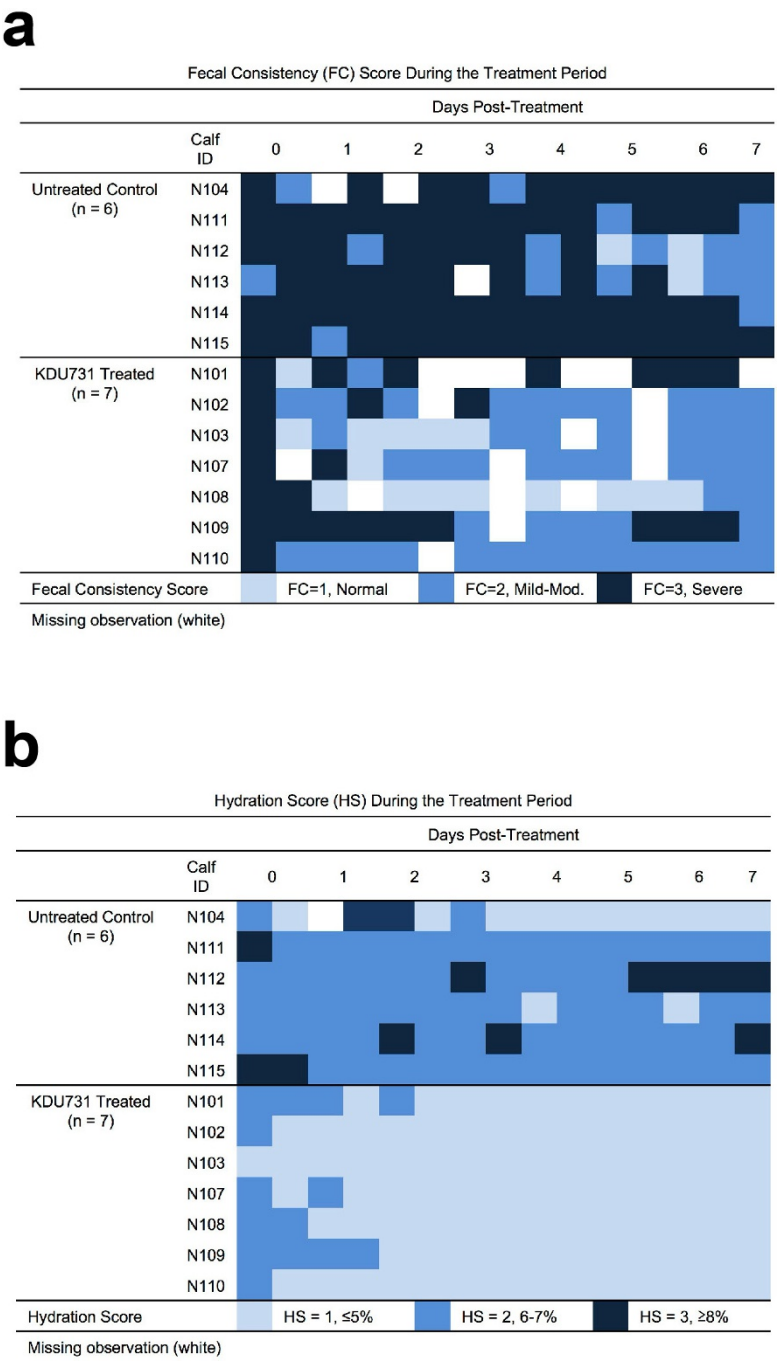

Extended Data Figure 7 | Effect of KDU731 on severity of diarrhoea and dehydration in the neonatal calf model of cryptosporidiosis. Severity of diarrhoea and dehydration in individual calves challenged with 5×10^7 *C. parvum* oocysts. Infected calves were treated with vehicle ($n = 6$) or with KDU731 ($n = 7$); n represents the number of calves. Every 12 h, calves were stimulated to defecate, faecal consistency was evaluated, and hydration status was assessed. Faecal consistency and hydration scores were assigned according to the study rubric (see Supplementary Information). The schematic representation shows the faecal consistency (**a**) and hydration scores (**b**) throughout the drug treatment period. Faecal consistency and hydration began to improve within 48 h of initiating treatment with KDU731.

© 2017 Macmillan Publishers Limited, part of Springer Nature. All rights reserved.

Extended Data Table 1 | Physicochemical properties and safety profiling data for KDU731

Properties	KDU731
Physicochemical	
Molecular Weight (Da)	396.41
Solubility (pH 6.8) (μM)	20
Lipophilicity (logP)	1.7
PAMPA (% calc fraction absorbed)	34.7
Caco2 permeability (ratio B-A/A-B)	2.42
In vitro clearance (M/R/D/Mk/H)	
Microsomal CLint [μl/min•mg]	50 / 29 / 36 / 39 / 13
Hepatocytes [μl/min/million cells]	- / 6 / < 0.6 / <4 / 12
Cellular activity (μM)	
Cytotoxicity HepG2 (CC_{50})	15.6
C. parvum / *C. hominis* (EC_{50})	0.10 / 0.13
HepG2 CC_{50} / *C. parvum* EC_{50} ratio (SI)	> 100
% Plasma protein binding	
M/R/D/H	- / 87.7 / 70.8 / 79.1
Human lipid and related kinase enzyme IC_{50} (μM)	
PI(4)β	1.4
PI(3)α	1
PI(3)β	1.9
PIK(3)Cγ	0.88
PIK(3)Cδ	0.39
VPS34	>9.1
mTOR	4.3
CYP P450 isoforms inhibition (IC_{50} μM)	
Reversible 3A4	>50
Reversible 2D6	>50
Reversible 2C9	>4.8
Time dependent inhibition 3A4	Negative
CYP induction, PXR functional assay	> 10
Cardiotoxicity	
hERG Binding (μM)	>30
Q-Patch IC_{50} (μM)	28
Patch Clamp Nav1.5 Quattro IC_{50} (μM)	>50
Genotoxicity	
Mini-AMES	Negative
Micronucleus test (MNT)	Negative
Phototoxicity (PIF values)	Negative (3.1)
Safety pharmacology profiling* (selected receptors, ion-channels, transporters, kinases etc)	No significant binding/inhibition

* Details in Extended Data Table 2. Data presented here is from assays repeated at least 2 times

© 2017 Macmillan Publishers Limited, part of Springer Nature. All rights reserved.

Extended Data Table 2 | Effect of KDU731 on radio-ligand binding to a panel of human recombinant receptors and pharmacologically relevant proteases/kinases

Binding assay*	IC_{50} (μM)
Adenosine 1 receptor	>30
Adenosine 2A receptor	>30
Adenosine 3 receptor	>30
Adenosine transporter	>30
Adrenergic ß1	>30
Adrenergic α2B receptor	>30
Adrenergic α2C receptor	>30
Angiotensin II AT1 receptor	>30
Benzodiazepine receptor †	>30
Cholecystokinin A receptor	>30
Cholecystokinin B receptor	>30
COX-1 assay ‡	>30
COX-2 assay	>30
Dopamine D2 receptor	>30
Dopamine D3 receptor	>30
Dopamine transporter	>30
Endothelin A receptor	>30
Ghrelin receptor	>30
Histamine H1 receptor	>30
Histamine H3 receptor	>30
Melanocortin MC3 receptor	>30
Monoamine oxydase A	>30
Motilin receptor	>30
Muscarinic M1 receptor	>30
Muscarinic M3 receptor	>30
Nicotinic (CNS) receptor	>30
NMDA channel site receptor	>30
Norepinephrine transporter	>30
Opiate δ receptor	>30
Opiate κ receptor	>30
Phosphodiesterase 3	>4.5
Phosphodiesterase 4D	>30
Serotonin 5-HT 2C receptor	>30
Serotonin 5-HT3 receptor	>30
Serotonin transporter	>30
Vasopressin V1a receptor	>30

Kinase assay	IC_{50} (μM)
cABLT315	>10
ALK	>10
Aurora-A K	>10
AXL	>10
BTK	>10
CDK2A	>10
CDK4D1	>10
EGFR	>10
EPHA4	>10
EPHB4	>10
FGFR3	>10
GSK3B	>10
IGF1R	>10
INSR	>10
JAK1	>10
JAK2	6.7
JAK3	>10
KDR	>10
KIT	>10
LCK	>10
MAP3K8	>10
MAPK14	>10
MAPK1	>10
MET	>10
PDGFRA	>10
PDPK1	>10
PKN1	>10
PKN2	>10
PRKCA	>10
PRKCQ	>10
RET	>10
ROCK2	>10
SYK	>10
TYK2	>10
ZAP70	>10
Protease assays	
Caspases 3	>30
Cathepsin D	>30
Matrix Metalloproteinases MMP08	>30
Thrombin	>30

*All human except †rat and ‡sheep
Assays were repeated at least twice

© 2017 Macmillan Publishers Limited, part of Springer Nature. All rights reserved.

Extended Data Table 3 | *In vivo* pharmacokinetic analysis of KDU731 in mice, rats, monkeys, and calves

Route	Parameter	Units	Mice		Rats		Rats TK*		Monkeys		Calves	
p.o.	Dose	mg/kg	2.3	24.7	2.3	21.3	30	100	3	10	5[a]	5[b]
	C_{max}	nM	406	2788	161	532	19168	28373	72	120	228[a]	341[b]
	AUC	nM*h	2306	22624	1844	5235	93026 (18x)	130979 (25x)	1620	2580	1909[a]	2011[b]
	$t_{1/2}$	hours	2.47	1.39	4.3	3.14	-	-	-	-	-	-
	F	%	37	34	23	7	-	-	9	4	-	-
	C_{max} d.n		177	113	70	25	638.9	283.7	24	12	45.6	68.2
	AUC d.n		1003	916	802	245.8	3100.9 (13x)	1309.8 (5x)	540	258	381.8	402.2
i.v.	Dose	mg/kg	5		2.5				0.3		-	
	V_{ss}	L/kg	1.12		2.15				2.1		-	
	CL	mL/min/kg	16		12.4				6.8		-	
	$t_{1/2}$	hours	1.06		3.3				4.7		-	

Mice, Rats, Monkeys and Calves n = 4, 4, 3 and 7 respectively.
C_{max}, maximum concentration achieved; AUC, area under curve (0-24 hours); $t_{1/2}$, half-life; F, percentage oral bioavailability; C_{max} d.n, dose-normalized C_{max}; AUC d.n, dose-normalized AUC; V_{ss}, steady state volume of distribution; CL, clearance; TK, toxicokinetic study.
p.o. denotes oral gavage formulated in 0.5% w/v methylcellulose and 0.5% w/v Polysorbate80 in water except for rats TK study.
i.v. denotes intravenous injection formulated in PEG300/D5W (3:1, v/v) for mice; Propylene Glycol / Tween 80 / Water (20:20:60, v/v) for rats and Methylpyrrolidone / PEG200 (10:90, v/v) for monkeys.
*Rats TK: day 1 TK analysis of KDU731 formulated in solid dispersion (SD) formulation as described in Methods section; numbers in parenthesis indicate the exposure multiples compared 21.3 mg per kg (body weight) suspension formulation.
Calves[a], day 1, first dose PK data with KDU731 5 mg per kg (body weight) twice daily, AUC is 0-12 h.
Calves[b], day 7, 13th dose PK data with KDU731 5 mg per kg (body weight) twice daily, AUC is 0-12 h.

© 2017 Macmillan Publishers Limited, part of Springer Nature. All rights reserved.